Can. J. Remote Sensing, Vol. 31, No. 1, pp. 122–131, 2005

Improved ship detection with airborne polarimetric SAR data

C. Liu, P.W. Vachon, and G.W. Geling

Abstract. The ship-detection performance that can be obtained from polarimetric synthetic aperture radar (SAR) data is compared with that obtained from single-channel SAR data. Statistical decision theory is used to define decision variables that quantify the tradeoff between the probability of missed detection and the probability of false alarm; performance is characterized by calculating receiver operating characteristics from single-channel and polarimetric SAR data by using likelihood ratio tests with the Neyman–Pearson criterion. It is shown that ship-detection performance obtained with polarimetric SAR data is improved compared with that obtained with single-channel SAR data. We also evaluate the results of these algorithms when applied to single-channel, dual-channel amplitude-only, dual-channel with amplitude and phase, and fully polarimetric SAR data of known ships. In this way, the relative improvement in ship-detection performance that is realized by using polarimetric information is quantified.

Résumé. On compare les améliorations obtenues au niveau de la performance dans la détection des navires suite à l'utilisation des données polarimétriques radar à synthèse d'ouverture (RSO) comparativement aux données RSO à bande unique. La théorie de décision statistique est utilisée pour définir des variables de décision qui permettent de quantifier le compromis à faire entre la probabilité de détection ratée et la probabilité de fausse alarme; la performance est caractérisée en calculant les caractéristiques de fonctionnement du récepteur à partir de données RSO en bande unique et polarimétriques en utilisant des tests de ratio de probabilité avec le critère Neyman-Pearson. Il est démontré que l'on peut améliorer la performance au plan de la détection des navires en utilisant des données polarimétriques RSO comparativement aux données RSO en bande unique. Nous évaluons également les résultats de ces algorithmes appliqués à des données à bande unique, à deux bandes avec l'amplitude seulement, à deux bandes avec l'amplitude et la phase, et polarimétriques de navires connus. De cette façon, il est possible de quantifier l'amélioration relative de la performance dans la détection des navires réalisée en introduisant l'information polarimétrique.
[Traduit par la Rédaction]

Introduction

Ship detection is a key requirement in the military, coastguard, fisheries, and commercial transportation sectors. Ship detection by synthetic aperture radar (SAR) has been studied extensively. For example, RADARSAT-1 is a single-channel C-band SAR with HH polarization (i.e., horizontal transmit, horizontal receive antenna polarization) that offers a tradeoff between spatial resolution and swath width (e.g., Raney et al., 1991); the best available resolution is nominally 8 m in range by 8 m in azimuth for single-look data in the fine-beam mode with a swath width of 50 km. The largest available swath width is 500 km, with a nominal resolution of 100 m in range by 100 m in azimuth. Ship detection using RADARSAT-1 data has been studied by a number of authors, often using a *K*-distribution clutter model with a constant false-alarm rate (CFAR) detector (e.g., Vachon et al., 1997; Crisp, 2004).

Existing spaceborne SARs are either single-polarization systems (e.g., RADARSAT-1 with HH and ERS-1 and ERS-2 with VV) or dual-polarized systems offering amplitude information only (e.g., ENVISAT, which offers HH–VV, VV–VH, or HH–HV modes). However, RADARSAT-2 will offer many more modes, including quad polarimetric (i.e., simultaneous HH, HV, VH, and VV). In this context, we consider data from the Environment Canada (EC) CV-580 polarimetric SAR system to quantify the improvement in ship-detection performance that can be achieved by using a polarimetric SAR rather than a single-channel or a multipolarized SAR system. The CV-580 C-band SAR can provide fully polarimetric data with a resolution of 6 m in range and 0.8 m in azimuth for single-look data, with a noise floor that is significantly lower than that of RADARSAT-1 (Livingstone et al., 1995). Ship detection with CV-580 SAR data has been studied with Cameron decomposition (Yeremy et al., 2001) and via the symmetric scattering characterization method (SSCM) (Touzi et al., 2004). The proportion of elementary scatterers in ship and ocean returns has also been investigated (Ringrose and Harris, 1999).

This paper addresses the degree to which ship-detection performance can be improved by using polarization information, rather than single-channel SAR data. Statistical decision theory is applied directly to the components of the scattering matrix to obtain a decision variable. For CV-580 data, the four complex components of the scattering matrix are used. For ENVISAT-type data, the two detected components would be used. The detection performance is estimated by using C-band data, acquired with the EC CV-580 SAR during

Received 31 March 2004. Accepted 14 September 2004.

C. Liu,[1] P.W. Vachon, and G.W. Geling. Defence R&D Canada – Ottawa, 3701 Carling Avenue, Ottawa, ON K1A 0Z4, Canada.

[1]Corresponding author (e-mail: Chen.Liu@drdc-rddc.gc.ca).

sea trials conducted by Defence R&D Canada (DRDC) – Ottawa. We consider single-channel, dual-channel amplitude-only, dual-channel with amplitude and phase, and fully polarimetric SAR data of known ships to establish the improvement in detector performance with the introduction of additional polarization information. The methodologies and algorithms developed for ship-detection performance estimation with airborne SAR data can be extended to spaceborne SARs, such as those carried by RADARSAT-1, ENVISAT, and RADARSAT-2, provided that a sufficient number of ship samples are obtained.

Methodology

Derivation of decision variables

A polarimetric SAR system alternately transmits horizontal (H) and vertical (V) polarized electromagnetic pulses from an antenna and measures both the horizontal (H) and vertical (V) polarized scattered fields. There are four combinations of incident and scattered electric fields, HH, HV, VH, and VV, which are often described mathematically by a 2 × 2 scattering matrix **S**, with components S_{HH}, S_{HV}, S_{VH}, and S_{VV}. An **S** matrix is measured for each sample element (i.e., pixel) in an image. The components of **S** can be written as either a matrix

$$\mathbf{S} = \begin{bmatrix} S_{HH} & S_{HV} \\ S_{VH} & S_{VV} \end{bmatrix} \tag{1}$$

or a vector

$$\boldsymbol{X} = [S_{HH}\, S_{HV}\, S_{VH}\, S_{VV}]^T \tag{2}$$

where the superscript T is the transpose operator.

The elements of **S** are complex random variables, which are not necessarily independent. For reciprocal media, $S_{HV} = S_{VH}$, but in practice these components may not be equal owing to, for example, system imperfections and system noise. The elements of **S** contain a common random phase factor that depends on the distance from the radar to the target.

For target detection, the target must be distinguished from the clutter background. In this case, the target is a ship, and the clutter background is the backscatter from the ocean surface. The ensembles of **S** matrices that make up the ship and the ocean are assumed to have different probability distributions. These distributions vary according to type of ship; ship motion; ship orientation; incidence angle; and environmental conditions, such as wind speed, wind direction, and wave height. If it is assumed that the ship and ocean samples are samples of random variables from two different probability distributions, then statistical decision theory can be applied to distinguish between the two.

The probability distributions of **S** are rather complicated functions. As a first approximation, **S** is considered to have a multivariate Gaussian distribution with zero mean. In practice, it is known that the ocean distribution is more heavily weighted toward larger intensities than a Gaussian distribution. For example, a *K*-distribution is often used to model the ocean clutter distribution for a single-channel SAR system (e.g., Vachon et al., 1997). In this work, we have also noted that ship scattering distributions also share this characteristic. Gaussian statistics will be used to determine the decision variable; measured data will be used to calculate the detection performance.

To apply statistical decision theory, it is assumed that both distributions are Gaussian. In practice, the distributions for both ocean and ships have more high-amplitude samples than a Gaussian distribution. This was seen from the cumulative distribution functions of the individual channels of the ship and ocean samples. Matching them to *K*-distributions was not attempted during this study, but deviations from Gaussian were evident at higher amplitudes, particularly from ship samples.

The variation of ship samples is, in principle, deterministic. However, a ship has many types of scattering features, and in this study, the number of ship samples was typically on the order of several hundred. Also, the scattering characteristics are affected by incidence angle, aspect angle, ship motion, and environmental conditions. Modelling ship samples by a probability distribution is therefore appropriate.

The key problem is to determine whether a particular image sample belongs to a ship or to the ocean. This is a binary decision for which four possible outcomes are considered here: a sample could be from the ocean and could be correctly detected; a sample could be from the ocean and could be falsely detected as a ship (a false alarm); a sample could be from a ship and could be correctly detected; or a sample could be from a ship and could be falsely detected as an ocean sample (missed detection). The optimum detector for this situation is a likelihood ratio test with the Neyman–Pearson criterion (Scharf, 1991), because the a priori probabilities of ship and ocean samples are unknown. This test maximizes the probability of detection, subject to the constraint that the probability of false alarm is less than a specified value (e.g., 10^{-6}).

In this test, a likelihood ratio (or a function of it) is formed from **S** and is compared with a threshold. If it exceeds the threshold, then the sample is determined to be from a ship; otherwise, it is determined to be from the ocean. The performance of the detector is characterized by a plot of the probability of detection, P_D, versus the probability of false alarm, P_{FA}, for various values of the detection threshold. This curve is commonly referred to as a receiver operating characteristic (Scharf, 1991). In this paper, we will consider the probability of missed detection $P_{MD} = 1 - P_D$ and define the receiver operating characteristic as P_{MD} versus P_{FA}. Such a graph contains the same information as P_D versus P_{FA}, but it is easier to interpret because P_D is often close to unity. Also, the probability of missed detection, P_{MD}, is one of the key quantities of interest.

Let U be a vector or matrix of measured variables for each sample of an image. For a sample belonging to a ship, the probability density function is $P_s(U)$. For a sample belonging to

the ocean, the probability density function is $P_o(U)$. Then, the likelihood ratio is defined as

$$L = \frac{P_s(U)}{P_o(U)} \tag{3}$$

and the likelihood ratio test is

$$L = \begin{cases} > \eta & \text{for a ship} \\ \leq \eta & \text{for ocean} \end{cases} \tag{4}$$

where η is a threshold. An equivalent form is to take the natural logarithm of L:

$$\ln L = \begin{cases} > \eta' & \text{for a ship} \\ \leq \eta' & \text{for ocean} \end{cases} \tag{5}$$

where $\eta' = \ln(\eta)$. Using $\ln(L)$ is equivalent to using L because $\ln(\cdot)$ is a monotonic function. Also, for Gaussian random variables, the ratio becomes a difference, and the number of mathematical operations required is reduced. The likelihood ratio is simplified to obtain a decision variable that minimizes the calculations required to analyze a large volume of data.

If the probability densities $P_s(U)$ and $P_o(U)$ are known, the optimum likelihood ratio can be formed, and in principle, the detector performance can be calculated for any threshold value. In practice, the densities are not known, and an exact performance calculation is not possible. To overcome this problem, the statistics of the scattering matrix elements are assumed to have a Gaussian distribution, and a decision variable with a reasonably simple mathematical form can then be calculated. Then, actual measured data from sea trials may be used to calculate the receiver operating characteristic for a number of cases. The use of measured data provides a realistic performance indication because it includes target, clutter, and other system effects.

A zero mean complex vector $\boldsymbol{X}$ that has a Gaussian distribution has a probability density function (Goodman, 1963; 1985) as follows:

$$P(\boldsymbol{X}) = \frac{1}{\pi^p |C|} \exp(-\boldsymbol{X}^H C^{-1} \boldsymbol{X}) \tag{6}$$

where $C = E(\boldsymbol{X}\boldsymbol{X}^H)$ is the covariance matrix; $E(\cdot)$ is the expectation operation over a region of the image; the parameter p is the number of elements in $\boldsymbol{X}$; $|\cdot|$ denotes a determinant; and H is the conjugate transpose operator. For four independent channels, as are available from a polarimetric SAR, the probability density function becomes

$$P(\boldsymbol{X}) = \frac{1}{\pi^4 \sigma_1^2 \sigma_2^2 \sigma_3^2 \sigma_4^2} \exp\left(-\frac{|x_1|^2}{\sigma_1^2} - \frac{|x_2|^2}{\sigma_2^2} - \frac{|x_3|^2}{\sigma_3^2} - \frac{|x_4|^2}{\sigma_4^2} \right) \tag{7}$$

where $\sigma_i^2 = E(|X_i|^2)$.

For a single-channel system, the probability density function is

$$P(X) = \frac{1}{\pi \sigma^2} \exp\left(-\frac{|x|^2}{\sigma^2} \right) \tag{8}$$

where X is a complex scalar. In Equations (6)–(8), any additive or multiplicative terms that do not contain the variable X may be absorbed into the threshold.

For a polarimetric SAR system with complex multivariate Gaussian densities for both ship and ocean, $\boldsymbol{X}$ is distributed according to Equation (6) with covariance matrices $\mathbf{C}_s$ and $\mathbf{C}_o$ for ship and ocean, respectively. The likelihood ratio of Equation (3) becomes, after taking logarithms and absorbing constant terms into the threshold,

$$\boldsymbol{X}^H (\mathbf{C}_o^{-1} - \mathbf{C}_s^{-1}) \boldsymbol{X} = \begin{cases} > \eta' & \text{for a ship} \\ \leq \eta' & \text{for ocean} \end{cases} \tag{9}$$

It is typically found that the elements of the covariance matrix for the ship samples are much larger in magnitude than those of the ocean samples. Then, Equation (9) can be approximated by

$$\boldsymbol{X}^H (\mathbf{C}_o^{-1}) \boldsymbol{X} = \begin{cases} > \eta' & \text{for a ship} \\ \leq \eta' & \text{for ocean} \end{cases} \tag{10}$$

In this approximation, the ship covariance matrix is not required.

Equations (9) and (10) can be applied to both quad polarimetric systems and dual polarimetric systems with amplitude and phase by using appropriate definitions of $\boldsymbol{X}$ and the covariance matrices. For a quad polarimetric system, $\boldsymbol{X}$ is defined in Equation (2); for a dual-channel system, $\boldsymbol{X}$ is a vector with two terms.

Some radar systems provide multipolarization amplitude information, such as HH–HV, VV–VH, or HH–VV. In this case, if the channels are initially assumed to be independent because the exact correlation information cannot be obtained from the measurements, the likelihood ratio of Equation (9) is then written as

$$\sum_{i=1}^{p} |X_i|^2 \left(\frac{1}{\sigma_{oi}^2} - \frac{1}{\sigma_{si}^2} \right) = \begin{cases} > \eta' & \text{for a ship} \\ \leq \eta' & \text{for ocean} \end{cases} \tag{11}$$

where $|X_i|$ is the amplitude of the complex variable X_i. This is approximately true for HH–HV, HH–VH, VV–HV, and VV–VH, so Equation (11) can be used for these cases. However, as the HH and VV channels are highly correlated for the ocean, Equation (11) must be modified to include cross-terms for the ocean. An approximate decision variable for a dual-polarized system derived from Equation (6) with two channels is

$$|X_1|^2\left(\frac{1}{\sigma_{o1}^2(1-\rho^2)}-\frac{1}{\sigma_{s1}^2}\right)+|X_2|^2\left(\frac{1}{\sigma_{o2}^2(1-\rho^2)}-\frac{1}{\sigma_{s2}^2}\right)$$

$$-\frac{2\rho}{1-\rho^2}\frac{|X_1|\cdot|X_2|}{\sigma_{o1}\sigma_{o2}}=\begin{cases}>\eta' & \text{for a ship}\\ \le\eta' & \text{for ocean}\end{cases} \qquad (12)$$

where ρ is the magnitude of the ocean correlation coefficient; and it is assumed that the ship variables are uncorrelated. Although only the magnitude of ρ is used here, estimation of this parameter requires both amplitude and phase information. Lee et al. (1994) also showed that ocean samples in general have a high correlation between HH and VV components. In addition, they showed that for circular Gaussian complex random variables, ρ can be obtained from the distributions of the magnitudes of the variables.

Performance estimation

We consider the estimation of detection performance by using measured data, which gives a realistic performance indication, as it includes target, clutter, and system effects. Areas of ocean samples and areas of ship samples having similar incidence angles are selected from an image. The covariance is estimated for each area separately, and the appropriate decision variable is formed.

The decision variable is then estimated for each ship sample and compared with a threshold. Those samples that are below the threshold are counted as missed detections. Similarly, the decision variable is calculated for each ocean sample and compared with the same threshold. Those samples that are above the threshold are counted as false alarms.

Let N_o be the total number of ocean samples considered, and let N_{FA} be the number of ocean samples detected as false alarms. Then, $P_{FA} = N_{FA}/N_o$. Similarly, let N_s be the total number of ship samples, and let N_{MD} be the number of missed detections. Then $P_{MD} = N_{MD}/N_s$. This procedure is repeated for various values of the decision threshold, which allows construction of the receiver operating characteristic, P_{MD} versus P_{FA}.

We now consider estimation of the error bar in our ship-detection performance curves. The accuracy of the estimated values of P_{MD} and P_{FA} may be determined from the number of missed-detection and false-alarm events. Let N_s be the number of ship samples, N_o be the number of ocean samples, P'_{MD} be the true probability of missed detection, and P'_{FA} be the true probability of false alarm. Assuming that both the ship and ocean samples are independent, the number of missed-detection events counted and the number of false-alarm events counted during the estimation procedure follow binomial distributions. The average number of missed-detection events is $N_sP'_{MD}$, and the standard deviation (SD) is $[N_sP'_{MD}(1-P'_{MD})]^{1/2}$. Similarly, the average number of false alarms is $N_oP'_{FA}$, and the SD is $[N_oP'_{FA}(1-P'_{FA})]^{1/2}$. Usually, $P'_{MD} << 1$ and $P'_{FA} << 1$, so the SDs are approximately $[N_sP'_{MD}]^{1/2}$ and $[N_oP'_{FA}]^{1/2}$.

If the samples are not independent, then the effective number of samples is smaller than the actual number of samples, which is the case for CV-580 data; the resolution is 6 m in range and 0.8 m in azimuth, whereas the pixel size is 4 m in range and 0.43 m in azimuth. Thus, the error levels may be higher than those derived above. For our purposes, the SD will be used as measure of the potential error. Here, the average number of counted events is taken to be the same as the actual number, which is a reasonable approximation because the objective is to obtain a rough estimate of the potential errors. The potential error levels must be taken into account when comparing performance curves.

Another source of error in using the measured data arises from the way in which the target is segmented from the surrounding ocean clutter to define the sets of samples that are designated as ship and ocean. In a SAR image, a ship appears as a localized region with higher intensity than the surrounding ocean. However, near the edge of the region containing the ship, it may not be clear whether a particular sample is part of the ship or part of the ocean. The number of ship samples is usually small (several hundred in the cases considered here with the CV-580 system; in general, the number of ship samples depends on the ship size and the sensor resolution), and it is desirable to maximize the number of samples to reduce the error levels caused by random variations. Furthermore, the covariance may not be the same for all parts of the ship, as different features on the ship may be resolved. We considered only samples that were well within the ship to ensure accurate estimation. On the other hand, the image is primarily composed of ocean samples, so only those well away from the ship need be used. This study used 2×10^6 ocean samples, and the number of ship samples ranged from 162 to 1086.

It should also be noted that some performance estimates assume that the ship and ocean statistics are known. This represents a best-case scenario and is used here because the objective is to determine how much improvement can be

Table 1. Ships considered and key parameters during data acquisition.

Line/pass, date	Ship	Length (m)	θ_{inc} (°)[a]	Wind speed (knots)[b]	Wave height (m)
3/1, 28 Mar 2000	HMCS *Ville de Québec*	135	37	20	4
3/1, 28 Mar 2000	M/V *Anne S. Pierce*	35	29	20	4
5/7, 30 Mar 2000	HMCS *Ville de Québec*	135	57	35	3–4
1/1, 7 Oct 2003	CFAV *Quest*	76	42	Calm	Calm

[a] θ_{inc}, incidence angle.
[b] 1 knot = 1.852 km/h.

obtained through the use of polarimetric data. A practical ship-detection method must resolve this issue.

Results and discussion

The methodology developed in the previous sections has been applied to several SAR images to determine the relative performance of different types of radar systems. The data used in this paper were acquired by the EC CV-580 SAR system during the Crusade trial in March 2000 and during the DRDC Ottawa Quest trial in October 2003. The Crusade trial was a joint experiment involving DRDC Ottawa and several other Canadian government organizations (Hawkins et al., 2001). Some key acquisition parameters for the data considered in this paper are summarized in **Table 1**.

An example of a multipolarized SAR ship image is shown in **Figure 1**, in which the magnitude of the HH channel is displayed in red, the magnitude of VV in blue, and the mean of the magnitudes of HV and VH in green. The corresponding performance estimates are shown in **Figures 2** and **3**, which include receiver operating characteristics for various types of radar systems. The results clearly show the advantage of the quad polarimetric system, which uses the amplitude and phase of all available data channels (triangles). Dual polarimetric systems provide better detection performance than single-channel systems. Various combinations of dual-channel systems with amplitude and phase (circles) and with amplitude only (squares), as well as single-channel systems (asterisks), are also included in **Figures 2** and **3**. We see that for single-channel systems in this example, HV or VH performs better than HH or VV, which is expected because the target-to-clutter ratios (TCRs) are higher for VH or HV than for HH or VV.

For completeness, the quad polarimetric case with amplitude only is also shown in **Figure 3**. In this case, it is assumed that the four channels are independent. The performance is seen to be better than that of any possible dual-channel system or single-channel system, except for an HH–VV dual-channel system with both amplitude and phase. It is also apparent that there are benefits to using the interchannel phase. In general, the detection performance improves as more information is introduced into the decision variable.

The detection performances estimated by considering both ship and ocean statistics (e.g., Equation (9)) are shown in **Figure 2**; those obtained by considering ocean statistics alone (e.g., Equation (10)) are shown in **Figure 3**. It is significant that the detection performances estimated with ocean statistics only (**Figure 3**) are essentially the same as those estimated with both

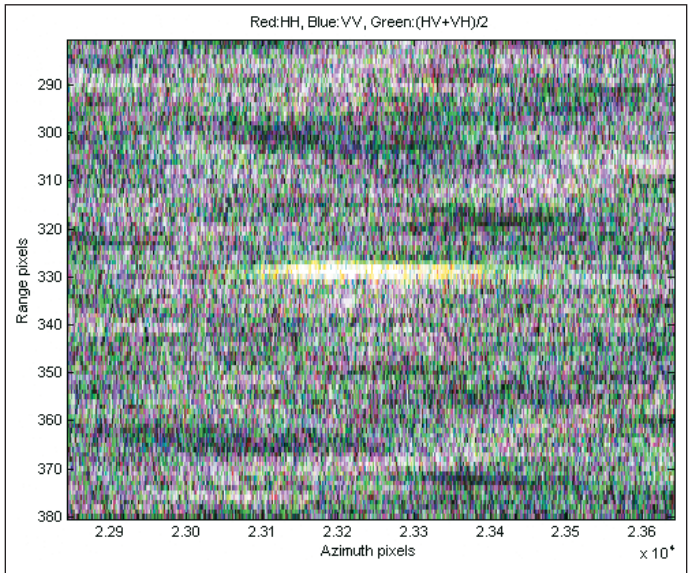

Figure 1. Polarimetric image of a ship on the ocean (HMCS *Ville de Québec*, line 3 pass 1, 28 Mar 2000).

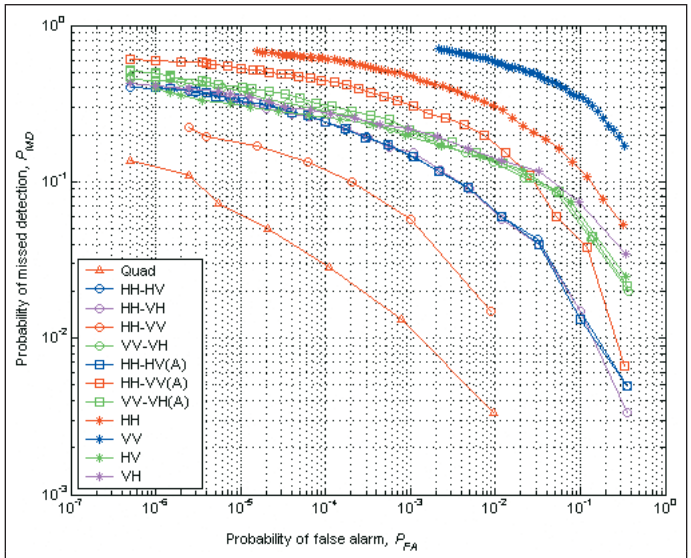

Figure 2. Detection performance with ocean and ship statistics (HMCS *Ville de Québec*, line 3 pass 1, 28 Mar 2000, $\theta_{inc} = 37°$, 603 ship pixels, 2×10^6 ocean pixels). θ_{inc}, incidence angle.

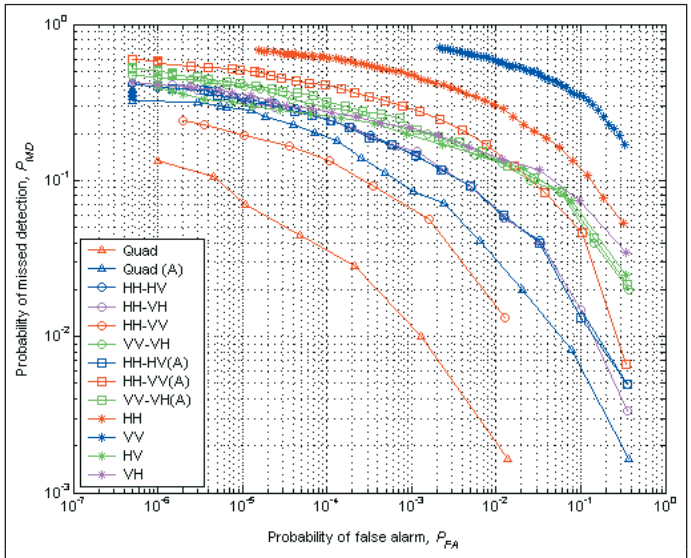

Figure 3. Detection performance with ocean statistics only (HMCS *Ville de Québec*, line 3 pass 1, 28 Mar 2000, $\theta_{inc} = 37°$, 603 ship pixels, 2×10^6 ocean pixels).

ocean and ship statistics (**Figure 2**). This observation forms the basis for developing practical ship-detection algorithms, as only ocean statistics are needed in the detection algorithm.

For these results, we used roughly 2×10^6 ocean samples and 162–1086 ship samples, corresponding to a minimum possible $P_{MD} = 6 \times 10^{-3}$ to 9×10^{-4} and $P_{FA} = 5 \times 10^{-7}$; a reasonable level of accuracy is achieved for $P_{MD} \geq 0.01$ and $P_{FA} \geq 10^{-6}$. **Figure 4** shows the variability in ship-detection performance for the fully polarimetric system of **Figure 3**, which is based on ocean statistics alone.

Figures 3 and **4** show detection performance curves for HMCS *Ville de Québec* at an incidence angle of $\theta_{inc} = 37°$. **Figures 5** and **6** show the corresponding curves for M/V *Anne S. Pierce* at $\theta_{inc} = 29°$. **Figures 7** and **8** show the detection performance curves for HMCS *Ville de Québec* at $\theta_{inc} = 57°$. **Figures 9** and **10** show the detection performance curves for CFAV *Quest* at $\theta_{inc} = 42°$.

Table 2 shows typical mean values for the **S** matrix elements and the mean TCR for the HMCS *Ville de Québec* at $\theta_{inc} = 37°$. **Table 3** gives the target-to-clutter ratios for all **S** matrix elements for all four cases illustrated in **Figures 2–10**.

Table 4 provides values of P_{MD} for $P_{FA} = 10^{-5}$ for our two HMCS *Ville de Québec* cases (**Figures 3** and **7**) at different incidence angles and for different environmental conditions. In each case, we have provided the estimated value of P_{MD}, as well as those values divided by the value of P_{MD}, for a fully polarimetric radar system. This table provides a concise

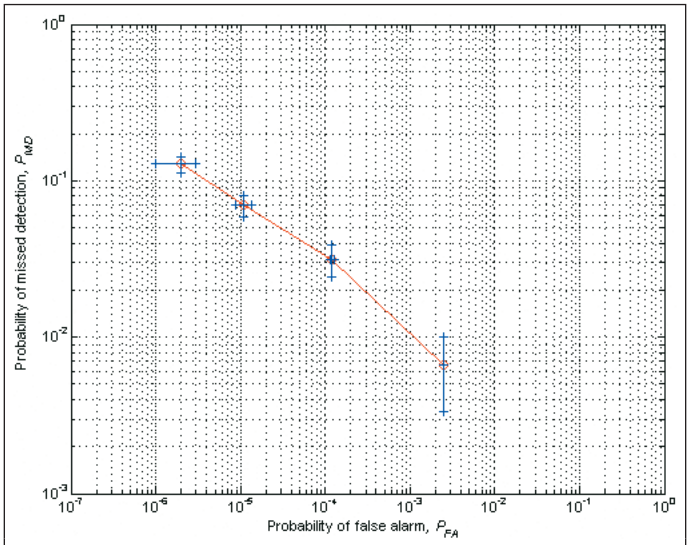

Figure 4. Quad polarization detection performance, with error bar estimates (HMCS *Ville de Québec*, line 3 pass 1, 28 Mar 2000, $\theta_{inc} = 37°$, 603 ship pixels, 2×10^6 ocean pixels).

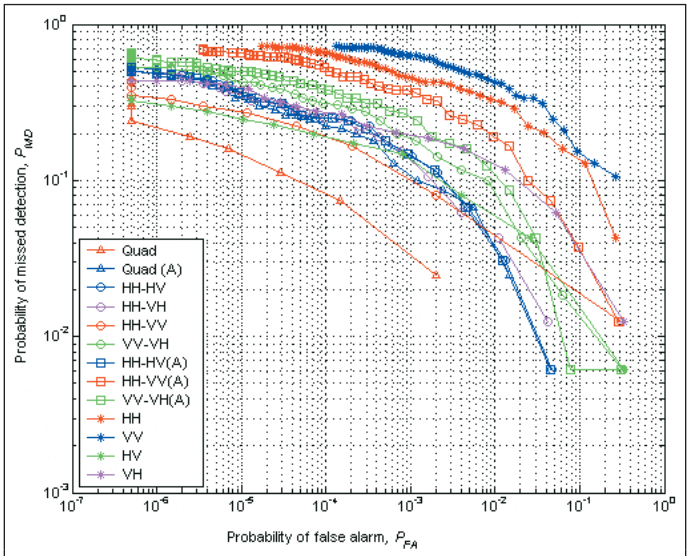

Figure 5. Detection performance with ocean statistics only (M/V *Anne S. Pierce*, line 3 pass 1, 28 Mar 2000, $\theta_{inc} = 29°$, 162 ship pixels, 2×10^6 ocean pixels).

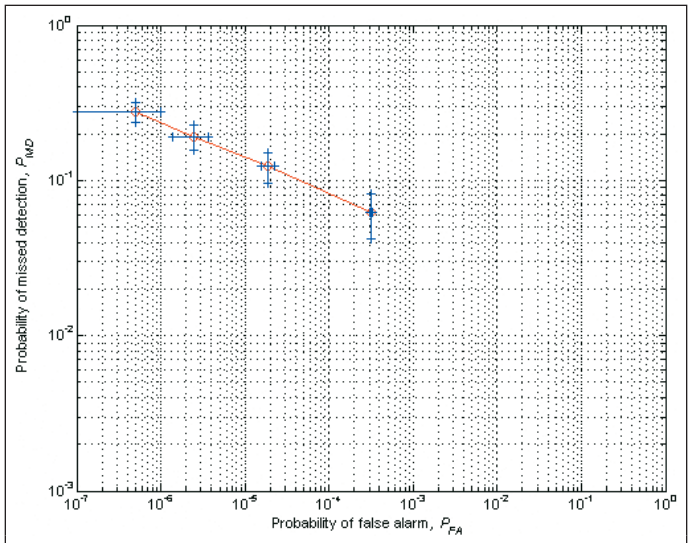

Figure 6. Quad polarization detection performance, with error bar estimates (M/V *Anne S. Pierce*, line 3 pass 1, 28 Mar 2000, $\theta_{inc} = 29°$, 162 ship pixels, 2×10^6 ocean pixels).

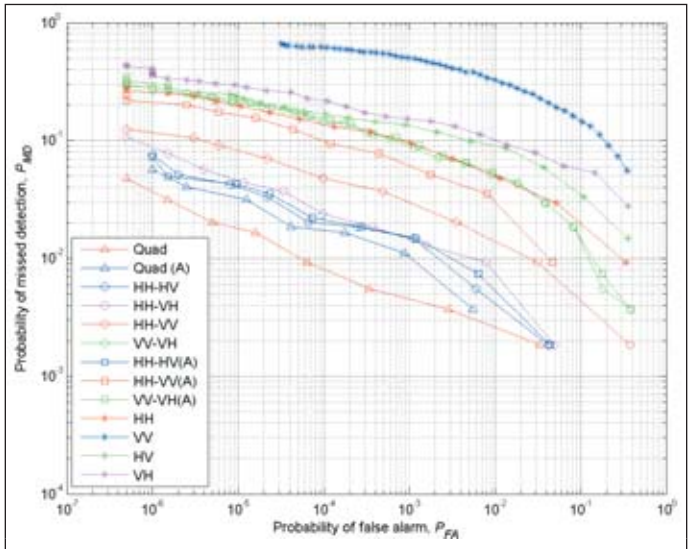

Figure 7. Detection performance with ocean statistics only (HMCS *Ville de Québec*, line 5 pass 7, 30 Mar 2000, $\theta_{inc} = 57°$, 540 ship pixels, 2×10^6 ocean pixels).

summary of the relative detection performance as illustrated by the plots of **Figures 3** and **7**.

The results of **Figures 3–10** and **Table 4** show that for the cases considered here, the quad polarimetric system always gives the best performance. Dual-channel systems with amplitude and phase generally provide better performance than dual-channel amplitude-only systems and single-channel systems. When the channels are uncorrelated, amplitude-only systems have the same performance as amplitude and phase systems.

The HH–VV amplitude and phase system often gives good performance, although it is not better than that of the quad polarimetric systems. This is consistent with the results of Lee et al. (2001), who considered classification of land targets with quad polarimetric, dual polarimetric, and single-channel systems at different frequencies. They showed that HH–VV systems give high classification accuracy under many conditions. A system having four channels with amplitude only (assuming that the channels are independent) also gives good detection performance.

The ship-detection performance of various radar systems as a function of incidence angle cannot be fully assessed from the data presented here. However, results for HMCS *Ville de Québec* are available for two incidence angles: 37° and 57°. For a quad polarimetric system, we see that the detection performance is better at $\theta_{inc} = 57°$.

Among the single-channel systems, the HV and VH systems have the best performance for two out of the four cases that have the lowest incidence angles. **Table 3** shows that for these cases, the TCR values are higher for the cross-polarized channels. For CFAV *Quest* at $\theta_{inc} = 42°$, all four channels have

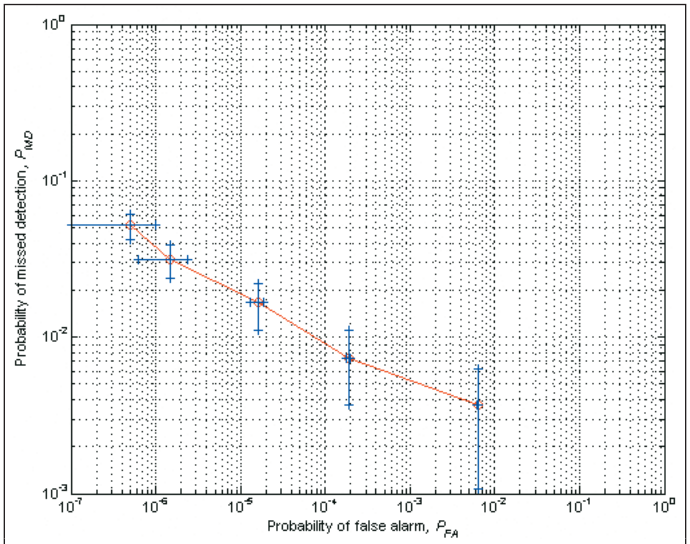

Figure 8. Quad polarization detection performance, with error bar estimates (HMCS *Ville de Québec*, line 5 pass 7, 30 Mar 2000, $\theta_{inc} = 57°$, 540 ship pixels, 2×10^6 ocean pixels).

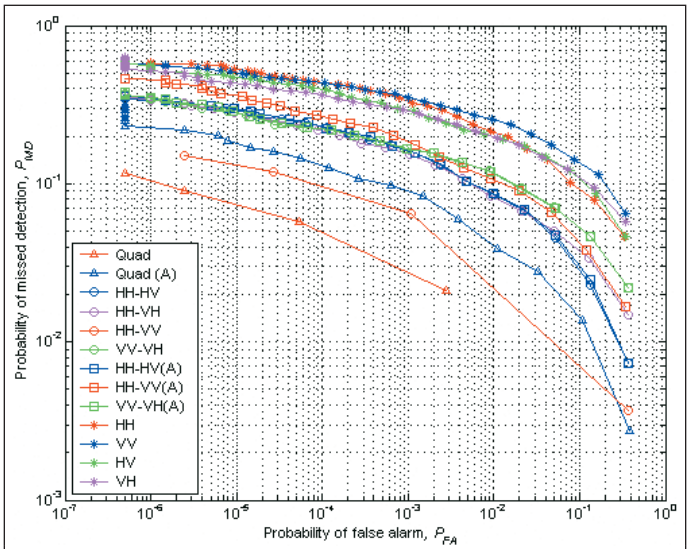

Figure 9. Detection performance with ocean statistics only (CFAV *Quest*, line 1 pass 1, 7 Oct 2003, $\theta_{inc} = 42°$, 1086 ship pixels, 2×10^6 ocean pixels).

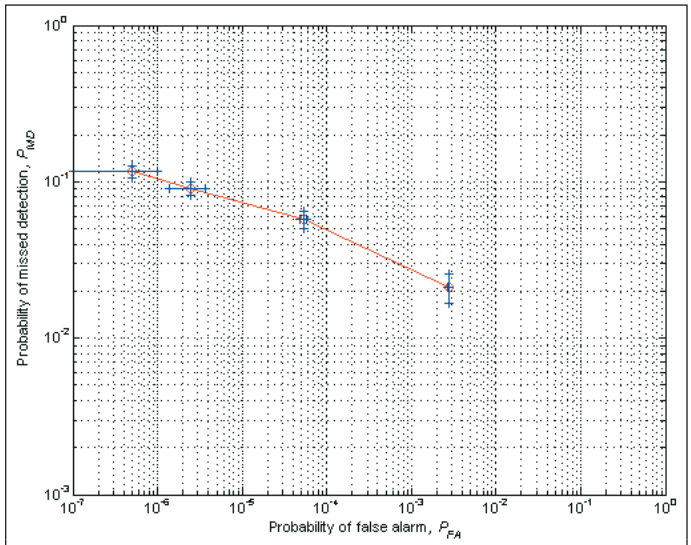

Figure 10. Quest polarization detection performance, with error bar estimates (CFAV *Quest*, line 1, pass 1, 7 Oct 2003, $\theta_{inc} = 42°$, 1086 ship pixels, 2×10^6 ocean pixels).

Table 2. Mean of ocean and ship and target-to-clutter ratio (HMCS *Ville de Québec*, line 3, pass 1, 28 March 2000).

	HH	HV	VH	VV
Mean intensity, ocean	1.52×10^{-2}	2.47×10^{-4}	2.72×10^{-4}	3.05×10^{-2}
Mean intensity, ship	4.49×10^{-1}	2.09×10^{-2}	1.92×10^{-2}	2.74×10^{-1}
Mean target-to-clutter ratio (dB)	1.47×10^{1}	1.93×10^{1}	1.85×10^{1}	9.54×10^{0}

Table 3. Target-to-clutter ratio for all cases.

Ship	θ_{inc} (°)[a]	HH	HV	VH	VV	No. of ship samples
M/V *Anne S. Pierce*	29	17.7	22.1	20.5	15.6	162
HMCS *Ville de Québec*	37	14.7	19.2	18.5	9.5	603
CFAV *Quest*	42	16.4	16.3	16.5	16.0	1086
HMCS *Ville de Québec*	57	20.4	17.9	16.7	11.5	542

[a] θ_{inc}, incidence angle.

Table 4. Values of P_{MD} for $P_{FA} = 10^{-5}$ for HMCS *Ville de Québec*.

	Line 3, pass 1, 28 Mar 2000		Line 5, pass 7, 30 Mar 2000	
Polarimetric system	P_{MD}	$P_{MD}/(7.53\times10^{-2})$	P_{MD}	$P_{MD}/(1.86\times10^{-2})$
Quad polarimetric	7.53×10^{-2}	1.00	1.86×10^{-2}	1.00
Quad (amplitude only)	2.88×10^{-1}	3.82	3.37×10^{-2}	1.81
HH–HV (amplitude and phase)	3.38×10^{-1}	4.49	4.11×10^{-2}	2.21
HH–VH (amplitude and phase)	3.34×10^{-1}	4.44	4.69×10^{-2}	2.52
HH–VV (amplitude and phase)	1.96×10^{-1}	2.60	8.53×10^{-2}	4.59
VV–VH (amplitude and phase)	4.01×10^{-1}	5.33	2.09×10^{-1}	11.23
HH–HV (amplitude only)	3.29×10^{-1}	4.37	4.22×10^{-2}	2.27
HH–VV (amplitude only)	5.09×10^{-1}	6.76	1.68×10^{-1}	9.03
VV–VH (amplitude only)	4.16×10^{-1}	5.52	2.21×10^{-1}	11.88
HH (single channel)	$>6.77\times10^{-1}$	>8.99	1.98×10^{-1}	10.65
VV (single channel)	$>7.03\times10^{-1}$	>9.34	$>6.61\times10^{-1}$	>35.53
HV (single channel)	3.11×10^{-1}	4.13	2.36×10^{-1}	12.69
VH (single channel)	3.59×10^{-1}	4.77	2.92×10^{-1}	15.70

Note: Incidence angles and environmental conditions are as indicated in **Table 1**.

Table 5. Absolute correlation coefficients of ocean and ship (HMCS *Ville de Québec*, line 3, pass 1, 28 Mar 2000).

	HH	HV	VH	VV
Ocean correlation				
HH	1.00	0.11	0.24	0.92
HV	0.11	1.00	0.84	0.11
VH	0.24	0.84	1.00	0.21
VV	0.92	0.11	0.21	1.00
Ship correlation				
HH	1.00	0.48	0.41	0.53
HV	0.48	1.00	0.98	0.57
VH	0.41	0.98	1.00	0.55
VV	0.53	0.57	0.55	1.00

similar performance, and the TCR values are similar as well. For HMCS *Ville de Québec* at $\theta_{inc} = 37°$, the cross-polarized channels are best; at $\theta_{inc} = 57°$, the HH channel is best. The HMCS *Ville de Québec* cases show that the TCR values decline for cross-polarized channels at higher incidence angles, whereas they increase for the co-polarized channels.

Table 5 gives absolute values of correlation coefficients for ship and ocean for the HMCS *Ville de Québec* at $\theta_{inc} = 37°$. **Table 6** gives the full complex correlation coefficients. HV and VH channels are highly correlated as expected. Also, HH and VV are highly correlated for the ocean samples. This is consistent with the findings of Lee et al. (1994). Most of the other correlation coefficients for the ocean are low, whereas for the ship they are in the vicinity of 0.5.

The phase angles between the HH and VV correlation coefficients give an indication of single-bounce or double-bounce scattering. For the ocean, the phase angle between HH and VV is about –38°; for the ship, it is about 126°. The ship samples therefore show evidence of double-bounce scattering.

Table 7 gives covariance matrices for the ship and ocean for HMCS *Ville de Québec* at $\theta_{inc} = 37°$. It can be seen that for ocean samples, the cross-polarized channels are much smaller in magnitude than the co-polarized channels. For ship samples, the cross-polarized channels are also smaller than the co-polarized channels, but not to the same extent as for the ocean samples. This results in higher cross-polarized TCR values, but this is not necessarily true for all incidence angles (see **Table 3**).

This analysis demonstrates that a fully polarimetric system gives the best ship-detection performance. This work will be extended to include an analysis of other datasets with different ships, different incidence angles, and different environmental conditions, to characterize performance under more general conditions.

Commercial spaceborne SAR systems generally have much coarser resolutions and poorer signal-to-noise ratios than the EC CV-580 SAR system considered in this paper. Nevertheless, the methodology and the ship-detection performance results of this paper are applicable to spaceborne systems. On first approximation, we expect the ship and ocean scattering

Table 6. Complex correlation coefficient of ocean and ship (HMCS *Ville de Québec*, line 3, pass 1, 28 Mar 2000).

	HH	HV	VH	VV
Ocean correlation				
HH	1.00×10^{0}	$-3.64\times10^{-2}-i\ 1.03\times10^{-1}$	$-3.88\times10^{-2}+i\ 2.34\times10^{-1}$	$7.24\times10^{-1}-i\ 5.70\times10^{-1}$
HV	$-3.64\times10^{-2}+i\ 1.03\times10^{-1}$	1.00×10^{0}	$8.42\times10^{-1}+i\ 1.33\times10^{-2}$	$3.57\times10^{-2}+i\ 1.03\times10^{-1}$
VH	$-3.88\times10^{-2}-i\ 2.34\times10^{-1}$	$8.42\times10^{-1}-i\ 0.13\times10^{-1}$	1.00×10^{0}	$-1.42\times10^{-1}-i\ 1.55\times10^{-1}$
VV	$7.24\times10^{-1}+i\ 5.70\times10^{-1}$	$3.57\times10^{-2}-i\ 1.03\times10^{-1}$	$-1.42\times10^{-1}+i\ 1.55\times10^{-1}$	1.00×10^{0}
Ship correlation				
HH	1.00×10^{0}	$3.44\times10^{-1}-i\ 3.27\times10^{-1}$	$3.49\times10^{-1}-i\ 2.07\times10^{-1}$	$-3.08\times10^{-1}+i\ 4.31\times10^{-1}$
HV	$3.44\times10^{-1}+i\ 3.27\times10^{-1}$	1.00×10^{0}	$9.81\times10^{-1}+i\ 1.09\times10^{-2}$	$-5.58\times10^{-1}+i\ 1.14\times10^{-1}$
VH	$3.49\times10^{-1}+i\ 2.07\times10^{-1}$	$9.81\times10^{-1}-i\ 1.09\times10^{-2}$	1.00×10^{0}	$-5.33\times10^{-1}+i\ 1.29\times10^{-1}$
VV	$-3.08\times10^{-1}-i\ 4.31\times10^{-1}$	$-5.58\times10^{-1}-i\ 1.14\times10^{-1}$	$-5.33\times10^{-1}-i\ 1.29\times10^{-1}$	1.00×10^{0}

Table 7. Covariance of ocean and ship (HMCS *Ville de Québec*, line 3, pass 1, 28 Mar 2000).

	HH	HV	VH	VV
Ocean covariance				
HH	1.52×10^{-2}	$-7.05\times10^{-5}-i\ 1.99\times10^{-4}$	$-7.87\times10^{-5}+i\ 4.73\times10^{-4}$	$1.55\times10^{-2}-i\ 1.22\times10^{-2}$
HV	$-7.05\times10^{-5}+i\ 1.99\times10^{-4}$	2.47×10^{-4}	$2.17\times10^{-4}+i\ 3.45\times10^{-6}$	$9.79\times10^{-5}+i\ 2.82\times10^{-4}$
VH	$-7.87\times10^{-5}-i\ 4.73\times10^{-4}$	$2.18\times10^{-4}-i\ 3.45\times10^{-6}$	2.70×10^{-4}	$-4.07\times10^{-4}-i\ 4.45\times10^{-4}$
VV	$1.55\times10^{-2}+i\ 1.22\times10^{-2}$	$9.79\times10^{-5}-i\ 2.82\times10^{-4}$	$-4.07\times10^{-4}+i\ 4.45\times10^{-4}$	3.04×10^{-2}
Ship covariance				
HH	4.49×10^{-1}	$3.33\times10^{-2}-i\ 3.17\times10^{-2}$	$3.25\times10^{-2}-i\ 1.93\times10^{-2}$	$-1.08\times10^{-1}+i\ 1.51\times10^{-1}$
HV	$3.33\times10^{-2}+i\ 3.17\times10^{-2}$	2.09×10^{-2}	$1.97\times10^{-2}+i\ 2.19\times10^{-4}$	$-4.22\times10^{-2}+i\ 8.65\times10^{-3}$
VH	$3.25\times10^{-2}+i\ 1.93\times10^{-2}$	$1.97\times10^{-2}-i\ 2.19\times10^{-4}$	1.92×10^{-2}	$-3.87\times10^{-2}+i\ 9.33\times10^{-3}$
VV	$-1.08\times10^{-1}-i\ 1.51\times10^{-1}$	$-4.22\times10^{-2}-i\ 8.65\times10^{-3}$	$-3.87\times10^{-2}-i\ 9.33\times10^{-3}$	2.74×10^{-1}

statistics for larger resolution cell sizes to be similar to those considered here, as the scattering mechanisms are identical.

Conclusions

This paper has studied the detection of ships with fully polarimetric SAR data by applying statistical decision theory to the polarimetric scattering matrix. Gaussian statistics were assumed to determine a decision variable, and performance was calculated with data from several sea trials acquired with the EC CV-580 SAR system. The detection performance was quantified by estimating receiver operating characteristics, which show the probability of missed detection (P_{MD}) as a function of the probability of false alarm (P_{FA}). These curves illustrate the tradeoff between P_{FA} and P_{MD}; a lower P_{FA} is accompanied by a higher P_{MD}.

We applied this methodology to several SAR images to calculate the performance of a number of different detector systems, including single channel, dual channel, and quad polarimetric. Amplitude-only and amplitude plus phase systems have also been considered. The results show that a fully polarimetric system is superior to all other single- and multi-polarization configurations. Dual-channel systems with amplitude and phase provide better detection performance than dual-channel amplitude-only systems and single-channel systems. However, when the channels are uncorrelated, amplitude-only systems have the same performance results as amplitude and phase systems (e.g., HH–HV, or VV–VH).

Future research will include tests with other datasets for various ships, incidence angles, and environmental conditions; study of ship motion effects on detection performance; and evaluation of the methodology and algorithms developed using airborne SAR data with ENVISAT and RADARSAT-1 and extension to RADARSAT-2. Multilook detection will also be studied, but the small number of ship samples may limit the ability to carry out ship-detection performance estimation.

The present work will be extended to implement a practical ship-detection algorithm for RADARSAT-2 polarimetric mode data. The issues to be resolved include selection of an appropriate decision variable and setting of the detection threshold. Equation (9) gives marginally better performance, but Equation (10) does not require any ship scattering statistics, which is a benefit because ship scattering statistics are not well known. The threshold would be chosen on the basis of the statistics of the decision variable for ocean samples and the required probability of false alarm.

For a practical spaceborne SAR for ship detection, the swath width must be maximized to cover as much area as possible. It is apparent that a RADARSAT-2 dual polarimetric mode (e.g., HH–VV with amplitude and phase) would provide better ship-detection performance than single-polarization modes, but across a broader swath than will be available from the quad polarimetric mode. Implementation of such a mode could be beneficial to the ship-detection sector.

Acknowledgements

We wish to thank the data acquisition and ground calibration teams from DRDC Ottawa, the Canada Centre for Remote Sensing, and Environment Canada; Terry Potter, for his assistance with the polarimetric data processing; and the reviewers, whose constructive comments helped us to improve this paper.

References

Crisp, D.J. 2004. In *The State-of-Art in Ship Detection in Synthetic Aperture Radar Image*. Defence Science and Technology Organization (DSTO) Information Science Laboratory, Edinburgh, Australia.

Goodman, J.W. 1963. Statistical analysis based on a certain multivariate complex Gaussian distribution (an introduction). *Annals of Mathematical Statistics*, Vol. 34, No. 152, pp. 152–180.

Goodman, J.W. 1985. *Statistical optics*. John Wiley & Sons, New York.

Hawkins, R.K., Murnaghan, K.P., Tennant, T., Yeremy, M., and Rey, M. 2001. Ship detection using airborne polarimetric SAR. In *CEOS SAR Workshop Proceedings*, 2–5 April 2001, Tokyo. CEOS-SAR01-032. NASDA/EORC, Tokyo. pp. 6–15.

Lee, J.-S., Hoppel, K.W., and Mango, S.A. 1994. Intensity and phase statistics of multilook polarimetric and interferometric SAR imagery. *IEEE Transactions on Geoscience and Remote Sensing*, Vol. 32, No. 5, pp. 1017–1028.

Lee, J.-S., Grunes, M.R., and Pottier, E. 2001. Quantitative comparison of classification capability: full polarimetric versus dual and single-polarization SAR. *IEEE Transactions on Geoscience and Remote Sensing*, Vol. 39, No. 11, pp. 2343–2351.

Livingstone, C., Gray, A., Hawkins, R., Vachon, P., Lukowski, T., and Lalonde, M. 1995. The CCRS airborne SAR systems: radar for remote sensing research. *Canadian Journal of Remote Sensing*, Vol. 21, No. 4, pp. 468–491.

Raney, R.K., Luscombe, A.P., Langham, E.J., and Ahmed, S. 1991. RADARSAT. *Proceedings of the IEEE*, Vol. 79, No. 6, pp. 839–849.

Ringrose, R., and Harris, N. 1999. Ship detection using polarimetric SAR data. In *CEOS SAR Workshop Proceedings*, 26–29 October 1999, Toulouse, France. ESA–CNES. pp. 687–691.

Scharf, L.L. 1991. *Statistical signal processing — detection, estimation, and time series analysis*. Addison-Wesley, Reading, Mass.

Touzi, R., Charbonneau, F., Hawkins, R.K., and Vachon, P.W. 2004. Ship detection and characterization using polarimetric SAR. *Canadian Journal of Remote Sensing*, Vol. 30, No. 3, pp. 552–559.

Vachon, P.W., Campbell, J.W.M., Bjerkelund, C.J., Dobson, F.W., and Rey, M.T. 1997. Ship detection by the RADARSAT SAR: validation of detection model predictions. *Canadian Journal of Remote Sensing*, Vol. 23, No. 1, pp. 48–59.

Yeremy, M., Campbell, J.W.M., Mattar, K., and Potter, T. 2001. Ocean surveillance with polarimetric SAR. *Canadian Journal of Remote Sensing*, Vol. 27, No. 4, pp. 328–344.